

## DEEP *SPITZER* OBSERVATIONS OF INFRARED-FAINT RADIO SOURCES: HIGH-REDSHIFT RADIO-LOUD ACTIVE GALACTIC NUCLEI?

RAY P. NORRIS<sup>1</sup>, JOSE AFONSO<sup>2,3</sup>, ANTONIO CAVA<sup>4</sup>, DUNCAN FARRAH<sup>5</sup>, MINH T. HUYNH<sup>6</sup>, R. J. IVISON<sup>7,8</sup>, MATT JARVIS<sup>9</sup>,  
MARK LACY<sup>10</sup>, MINNIE MAO<sup>1,6,11,12</sup>, CLAUDIA MARASTON<sup>13</sup>, JEAN-CHRISTOPHE MAUDUIT<sup>6</sup>, ENNO MIDDELBERG<sup>14</sup>, SEB OLIVER<sup>5</sup>,  
NICK SEYMOUR<sup>15</sup>, AND JASON SURACE<sup>6</sup>

<sup>1</sup> CSIRO Australia Telescope National Facility, P.O. Box 76, Epping, NSW, 1710, Australia, email: Ray.Norris@csiro.au

<sup>2</sup> Observatório Astronómico de Lisboa, Faculdade de Ciências, Universidade de Lisboa, Tapada da Ajuda, 1349-018 Lisbon, Portugal

<sup>3</sup> Centro de Astronomia e Astrofísica da Universidade de Lisboa, 1349-018 Lisbon, Portugal

<sup>4</sup> Departamento de Astrofísica, Facultad de CC. Físicas, Universidad Complutense de Madrid, E-28040 Madrid, Spain

<sup>5</sup> Astronomy Centre, Department of Physics & Astronomy, University of Sussex, Brighton BN1 9QH, UK

<sup>6</sup> Infrared Processing and Analysis Center, MS220-6, California Institute of Technology, Pasadena, CA 91125, USA

<sup>7</sup> UK Astronomy Technology Centre, Royal Observatory, Blackford Hill, Edinburgh EH9 3HJ, UK

<sup>8</sup> Institute for Astronomy, University of Edinburgh, Blackford Hill, Edinburgh EH9 3HJ, UK

<sup>9</sup> Centre for Astrophysics, Science & Technology Research Institute, University of Hertfordshire, Hatfield, Herts, AL10 9AB, UK

<sup>10</sup> NRAO, 520 Edgemont Road, Charlottesville, VA 22903, USA

<sup>11</sup> School of Mathematics and Physics, University of Tasmania, Private Bag 37, Hobart, 7001, Australia

<sup>12</sup> Anglo-Australian Observatory, P.O. Box 296, Epping, NSW, 1710, Australia

<sup>13</sup> Institute of Cosmology and Gravitation, Dennis Sciama Building, Burnaby Road, Portsmouth, PO1 3FX, UK

<sup>14</sup> Astronomisches Institut, Ruhr-Universität Bochum, Universitätsstr. 150, 44801 Bochum, Germany

<sup>15</sup> Mullard Space Science Laboratory, UCL, Holmbury St Mary, Dorking, Surrey, RH5 6NT, UK

Received 2010 April 6; accepted 2011 May 4; published 2011 July 6

### ABSTRACT

Infrared-faint radio sources (IFRSs) are a rare class of objects which are relatively bright at radio wavelengths but very faint at infrared and optical wavelengths. Here we present sensitive near-infrared observations of a sample of these sources taken as part of the *Spitzer* Extragalactic Representative Volume Survey. Nearly all the IFRSs are undetected at a level of  $\sim 1 \mu\text{Jy}$  in these new deep observations, and even the detections are consistent with confusion with unrelated galaxies. A stacked image implies that the median flux density is  $S_{3.6\mu\text{m}} \sim 0.2 \mu\text{Jy}$  or less, giving extreme values of the radio-infrared flux density ratio. Comparison of these objects with known classes of object suggests that the majority are probably high-redshift radio-loud galaxies, possibly suffering from significant dust extinction.

*Key words:* galaxies: evolution – galaxies: formation – galaxies: starburst

*Online-only material:* color figure

### 1. INTRODUCTION

Infrared-faint radio sources (IFRSs) are a rare class of objects which are relatively strong at radio wavelengths but very faint at infrared (IR) and optical wavelengths. They were first categorized in the Australia Telescope Large Area Survey (ATLAS; Norris et al. 2006) as radio sources with no observable IR counterpart in the co-spatial *Spitzer* Wide-area IR Extragalactic (SWIRE) Survey (Lonsdale et al. 2004). Most have flux densities of a few hundred  $\mu\text{Jy}$  at 20 cm, but some are as bright as 20 mJy. They may be related to the optically invisible radio sources found by Higdon et al. (2005, 2008), which are compact radio sources with no optical counterpart to  $R \sim 25.7$ , although the IFRSs seem even more extreme than the Higdon objects. Norris et al. (2006) and Middelberg et al. (2008b) have identified 51 such sources out of 2002 radio sources in the ATLAS survey.

So far, four samples of IFRSs have been identified: (1) the original ATLAS/SWIRE samples identified by Norris et al. (2006) and Middelberg et al. (2008b), from which the sources in this paper are drawn, (2) the sample in the *Spitzer* First Look Survey (FLS), identified by Garn & Alexander (2008), (3) the sample in ELAIS-N1 identified by Banfield et al. (2011), and (4) a sample in the COSMOS field (Scoville et al. 2007) identified by Zinn et al. (2011). These samples imply a sky density of  $\sim 7 \text{ deg}^{-2}$  for  $S_{20\text{cm}} > 0.1 \text{ mJy}$ .

At the time of their discovery, the IFRSs were unexpected, as SWIRE was thought to be deep enough to detect all extragalactic

radio sources at  $z \lesssim 2$ , regardless of whether star formation or active galactic nuclei (AGNs) powered the radio emission. Possible explanations were that these sources are (1) high-redshift radio-loud AGNs, (2) very obscured radio galaxies at more moderate redshifts ( $1 < z < 2$ ), (3) lobes of nearby but unidentified radio galaxies, (4) very obscured, luminous starburst galaxies, such as high-redshift submillimeter-selected galaxies (SMGs; Smail et al. 1997), (5) high-latitude pulsars, or (6) an unknown type of object. Of course it is also possible that they do not constitute a homogeneous class and harbor examples of some or all of the above.

The nature of IFRSs has been hard to determine because nearly all the information on them has been obtained at radio wavelengths. Spectroscopy is difficult because the hosts are optically faint and the radio positions can also have uncertainties of the order of a few arcsec. Norris et al. (2006) stacked the positions of 22 IFRSs in the *Spitzer* 3.6  $\mu\text{m}$  IRAC images and found no detection in the averaged image, showing that they are well below the SWIRE detection threshold. This was a surprising result at the time, as it was expected that the IFRSs represented the tail of a distribution reaching just below the SWIRE detection threshold, but it was confirmed by Garn & Alexander (2008) and by the new data presented here.

Middelberg et al. (2008a) and Norris et al. (2007) targeted six IFRSs with the Australian Long Baseline Array (LBA) and detected two of the sources. The Norris et al. (2007) LBA detection constrained the source size to less than 0.03 arcsec,

suggesting a compact radio core, powered by an AGN. Middelberg et al. (2008a) found the size and radio luminosity of their LBA-detected source to be consistent with a high-redshift ( $z > 1$ ) compact, steep-spectrum (CSS) source. The VLBI detections rule out the possibility that these particular IFRSs are simply the radio lobes of unidentified radio galaxies, or star-forming galaxies, though the initial VLBI targets were inevitably among the most radio-bright examples in the sample.

Garn & Alexander (2008) stacked IFRS sources in the *Spitzer* FLS at infrared wavelengths, as well as at 610 MHz. The sources they find in the FLS are very similar to the sources described here. They find that the IFRS sources can be modeled as compact Fanaroff Riley type II (FR II) radio galaxies at high redshift ( $z \gtrsim 4$ ), and argue that IFRSs are predominately high-redshift radio-loud AGNs.

Huynh et al. (2010) used deep data from the *Spitzer* IRAC MUSYC Public Legacy in E-CDFS (SIMPLE) project and the Far-Infrared Deep Extragalactic Legacy (FIDEL) *Spitzer* survey to probe more deeply in the E-CDFS region, and detected two of the four IFRSs in that region. However, the two non-detections, and the faintness of the two detected sources, enabled Huynh et al. to place constraints on the sources. Their detailed modeling of their spectral energy distributions shows that they are consistent with high-redshift ( $z > 1$ ) AGNs. They also noted that the ratio of 20 cm flux density,  $S_{20\text{cm}}$ , to  $3.6\ \mu\text{m}$  flux density,  $S_{3.6\ \mu\text{m}}$ , is higher than that of the general radio source population and has significant overlap with the population of high-redshift radio galaxies (HzRGs) investigated previously with *Spitzer* observations (Seymour et al. 2007) and is also consistent with the radio galaxy  $K-z$  relation extended to high redshifts (Jarvis et al. 2001; De Breuck et al. 2002; Willott et al. 2003).

Middelberg et al. (2011) have measured the spectral indices of the radio emission at several wavelengths of a sample of 17 strong IFRSs and find that they are significantly different from the general radio source population, and also different from the general AGN population. The spectra are steep, typically with  $\alpha \sim -1$ , and there is a particularly prominent lack of sources with  $\alpha > -0.7$  (where  $S_\nu \propto \nu^\alpha$ ). Banfield et al. (2011) also reported steep spectral indices, and both Middelberg et al. (2011) and Banfield et al. (2011) found that several of the IFRSs were significantly polarized, suggesting an AGN rather than a star-forming galaxy.

Each of these papers adds to a consensus view that the IFRSs represent a class of high-redshift radio-loud galaxies. However, there is not yet unequivocal evidence for this, and it is possible that the IFRS class constitutes several different types of objects.

Here, we present near-IR data taken as part of the *Spitzer* Extragalactic Representative Volume Survey (SERVS) project (Mauduit et al. 2011), which uses the data taken during the *Spitzer* warm mission to probe extended regions of the sky to a sensitivity some five times deeper than SWIRE. The SERVS project includes several square degrees around the ELAIS-S1 and CDFS extended fields in which IFRSs were detected as part of the ATLAS radio survey. These deeper data provide much tighter constraints on the nature of IFRSs.

Throughout this paper we assume a Hubble constant of  $71\ \text{km s}^{-1}\text{Mpc}^{-1}$ , and matter and cosmological constant density parameters of  $\Omega_M = 0.27$  and  $\Omega_\Lambda = 0.73$ .

## 2. OBSERVATIONS AND ANALYSIS

The ATLAS radio survey is still in progress, covering  $7\ \text{deg}^2$  at 20 cm in two regions, surrounding the CDF-S and ELAIS-S1

fields to an rms depth of typically  $10\ \mu\text{Jy beam}^{-1}$ . However, all the radio data used in this paper are taken from the preliminary ATLAS catalogs (Norris et al. 2006; Middelberg et al. 2008b) which surveyed the entire region to an rms depth of typically  $20\text{--}30\ \mu\text{Jy beam}^{-1}$ .

SERVS (Mauduit et al. 2011) is a medium-deep survey at  $3.6\ \mu\text{m}$  and  $4.5\ \mu\text{m}$  which exploits the warm phase mission of *Spitzer*, to cover an  $18\ \text{deg}^2$  field, which includes most of the ATLAS fields.

For the work described in this paper, we used SERVS data in the CDFS and ELAIS-S1 fields. Only band 1 (at  $3.6\ \mu\text{m}$ ) of the SERVS data was used because it is intrinsically more sensitive for most galaxy spectral energy distributions than the band 2 ( $4.5\ \mu\text{m}$ ) data. Figure 1 shows the IR and radio coverage of these fields. The SERVS data on the CDFS area covers nearly all of the area observed by SWIRE and ATLAS, but the ELAIS-S1 coverage is offset from the center of the SWIRE/ATLAS field by about a degree. Nevertheless, a total of 39 IFRSs are common to both data sets and are listed in Table 1.

For each IFRS source detected at radio wavelengths, we took the initial positional uncertainty ( $\delta_i$ , in R.A. and decl.) from the values listed by Norris et al. (2006) and Middelberg et al. (2008b), which were calculated from the quadrature sum of the formal fitting uncertainty and a 0.1 arcsec potential uncertainty in the position of the calibration source. We also consider the formal positional uncertainty due to noise  $\delta_{\text{noise}} = 0.3 \times \theta_b \times (S_{\text{rms}}/S_{\text{peak}})$ , where  $\theta_b$  is the synthesized full width half-maximum beamwidth,  $S_{\text{rms}}$  is the local rms flux density, and  $S_{\text{peak}}$  is the peak flux density of the source, as discussed by Ivison et al. (2007). We further considered any positional accuracy of less than 1 arcsec to be unrealistic because of systematic offsets and intrinsic source sizes. We derive a final  $3\sigma$  positional uncertainty  $\delta_{\text{final}}$  in R.A. and decl. as being the maximum of  $3 \times \delta_i$ ,  $3 \times \delta_{\text{noise}}$ , and 1 arcsec. These positional uncertainties are listed in Table 1.

For each IFRS source, we examined the SERVS  $3.6\ \mu\text{m}$  data for sources visible by eye as a distinct peak above the noise which fell within the error ellipse. Using this technique, we found that 3 of the 39 IFRS sources contained a  $3.6\ \mu\text{m}$  candidate source within the  $3\sigma$  radio position error ellipse. Images of two representative IFRSs are shown in Figure 2.

We then performed aperture photometry on each of these candidates. The flux density was measured using an aperture radius of 1.9 arcsec, which was found to be optimal in SWIRE. An aperture correction of 1.4 was applied for this radius (Surace et al. 2005). The uncertainty in the aperture flux density was estimated by measuring the rms of 100 randomly placed apertures placed near the source. The resulting flux densities are listed in Table 1.

The rms noise of the SERVS data, measured in a region of sky free from visible sources, can approach  $\sim 0.2\ \mu\text{Jy}$ . However, since SERVS data are typically confusion limited, such an rms can be misleading if used to calculate uncertainties. Instead, we placed 1000 random apertures across the image and followed an iterative approach, rejecting apertures with a flux density  $\gtrsim 2.5\sigma$  and recalculating the rms until the process converged. The rms thus obtained was  $0.51\ \mu\text{Jy}$  in the ELAIS-S1 field and  $0.64\ \mu\text{Jy}$  in the CDF-S field.

As the SERVS data approach the confusion limit of *Spitzer*, it is necessary to estimate how many of the candidate cross-identifications are due to confusion. We estimated this in two independent ways.

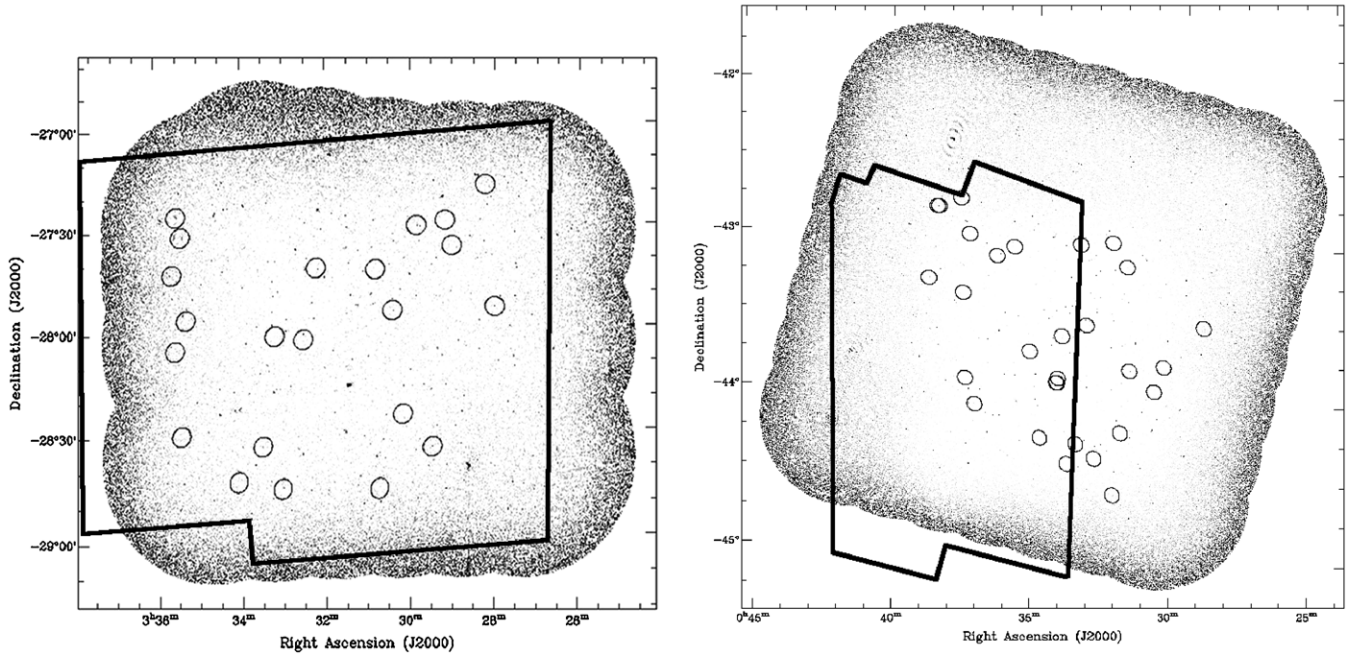


**Figure 1.** Field coverage of the data presented here. The left-hand image shows the region surrounding the CDFS field, while the right-hand image shows the ELAIS-S1 image. The gray scale shows the radio images, taken from Norris et al. (2006) and Middelberg et al. (2008b) and the circles show the positions of the IFRSs. The solid lines show the SERVS coverage. The 39 sources discussed in this paper, and listed in Table 1, are those shown here which also lie within the SERVS coverage.

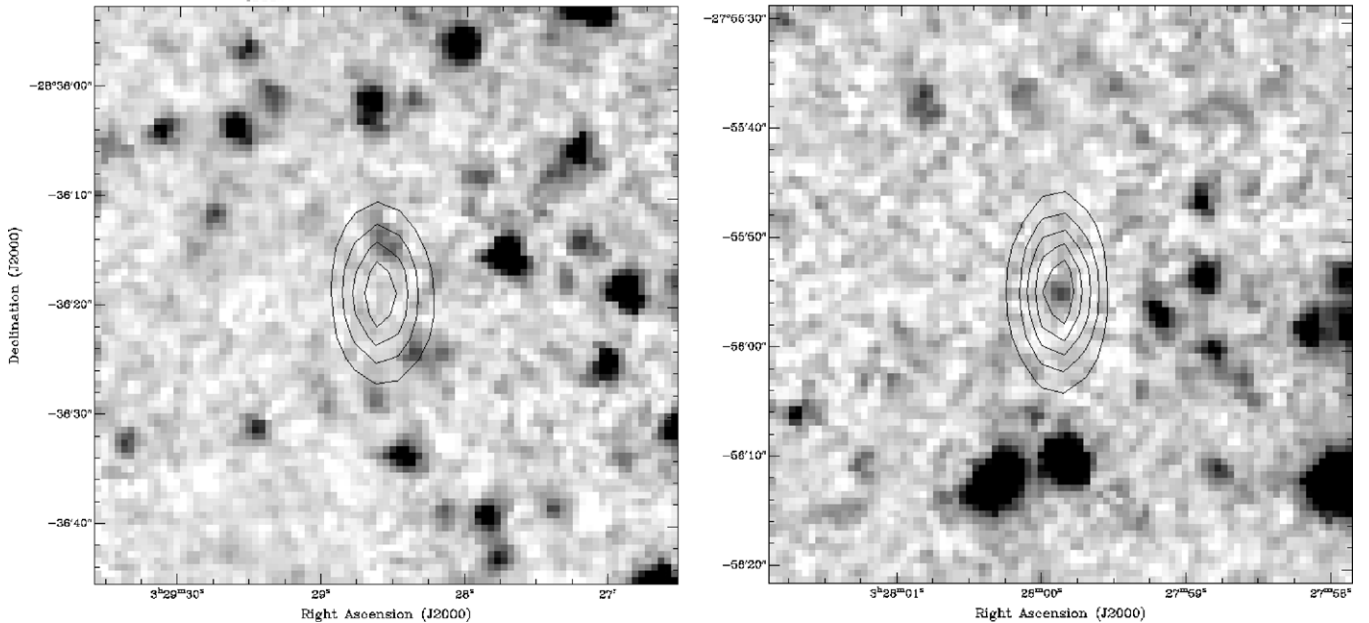


**Figure 2.** Two representative IFRS sources. The gray scale is the  $3.6\mu\text{m}$  SERVS data, and the contours are the 20 cm image, with contour levels of (1, 2, 3, 4, 5)  $\text{mJy beam}^{-1}$ . The left hand image is a non-detection (CS0194) and the right-hand image is a candidate detection (CS0114).

Our most reliable estimate was obtained by shifting the IFRS radio positions by an arbitrary amount (typically  $\sim 20$  arcsec) which is much greater than the beamsize of either the radio or IR data, but much smaller than the scale size of variations in the image sampling. We then examined the image to estimate how many IR sources fall by chance within the error ellipse. This is a very robust way of estimating the confusion, as it builds in the varying error ellipse size, and the non-uniform sensitivity, using the real data rather than a parameterized representation. Because it uses real data, with exactly the same process in both cases, it is immune to calibration or other systematic errors.

We then repeated this process 10 times, shifting the positions by a different amount ( $< 1$  arcmin in all cases). A mean of  $2.1 \pm 1.2$  of the shifted error ellipses contained a peak in the *Spitzer* data. Thus, of our three candidate identifications with unshifted data, we expect that 2.1 of these are due to confusion, leaving only zero or one genuine detection.

As a check on this result, we use the source counts calculated by Barmby et al. (2008). Our radio position error ellipses have a total area of  $266 \text{ arcsec}^2$ , and we have found three candidate identifications within this area, all of which are brighter than a flux density limit of  $\sim 1.1 \mu\text{Jy}$ . Barmby et al.

**Table 1**  
Radio and Infrared Flux Densities of the Infrared-faint Radio Sources

ID	Long Name	err(R.A.) (arcsec)	err(Decl.) (arcsec)	S(20 cm) (mJy)	S(3.6 $\mu$ m) ( $\mu$ Jy)	Notes
ES0011	AELAIS J003207.44-443957.8	1.21	1.00	1.67	out	
ES0056	AELAIS J003346.75-442902.8	1.00	1.17	0.58	<	
ES0079	AELAIS J003248.60-442625.7	1.18	1.22	0.31	out	
ES0135	AELAIS J003330.12-442115.4	1.59	1.55	0.18	<	
ES0190	AELAIS J003155.15-441610.4	1.38	1.79	0.27	out	
ES0318	AELAIS J003705.54-440733.6	1.00	1.12	1.59	<	
ES0407	AELAIS J003045.75-435926.3	1.00	1.00	0.65	out	
ES0427	AELAIS J003411.59-435817.0	1.00	1.00	21.36	<	VLBI source: see Middelberg et al. (2008b)
ES0433	AELAIS J003413.43-435802.4	1.00	1.00	0.25	<	
ES0436	AELAIS J003726.34-435733.0	1.07	1.53	0.19	<	
ES0463	AELAIS J003410.14-435625.5	1.23	1.75	0.14	<	
ES0509	AELAIS J003138.63-435220.8	1.00	1.00	22.20	out	Polarized source: see Middelberg et al. (2011)
ES0548	AELAIS J003027.04-434948.3	1.14	1.62	0.31	out	
ES0593	AELAIS J003510.80-434637.2	1.20	1.72	0.17	<	
ES0696	AELAIS J003402.26-434008.5	1.00	1.00	0.49	<	
ES0743	AELAIS J003311.40-433547.3	1.06	1.51	0.16	out	
ES0749	AELAIS J002905.22-433403.9	1.00	1.00	7.01	out	
ES0913	AELAIS J003733.42-432453.4	1.00	1.00	0.68	<	
ES0973	AELAIS J003844.13-431920.4	1.30	1.43	9.14	<	Polarized source: see Middelberg et al. (2011)
ES1056	AELAIS J003446.40-441926.9	1.00	1.40	0.37	<	
ES1083	AELAIS J003150.17-431235.2	1.00	1.35	0.22	out	
ES1118	AELAIS J003622.25-431015.0	1.04	1.49	0.51	<	
ES1154	AELAIS J003546.92-430632.4	1.00	1.08	0.53	<	
ES1170	AELAIS J003327.96-430439.8	1.00	1.26	0.42	out	
ES1180	AELAIS J003219.77-430315.6	1.00	1.00	0.50	out	
ES1193	AELAIS J003719.58-430201.4	1.05	1.51	0.23	<	
ES1259	AELAIS J003827.17-425133.7	1.00	1.00	4.52	<	
ES1260	AELAIS J003824.94-425137.9	1.30	1.85	0.80	<	
ES1275	AELAIS J003739.09-424814.0	1.33	1.90	0.46	out	
CS0114	ATCDF5 J032759.89-275554.7	1.00	1.00	7.17	$2.2 \pm 0.54$	VLBI source: see Norris et al. (2007)
CS0122	ATCDF5 J032812.99-271942.6	1.41	3.58	0.46	<	
CS0164	ATCDF5 J032900.20-273745.7	1.00	1.24	1.21	<	
CS0173	ATCDF5 J032909.66-273013.7	1.41	3.76	0.35	$2.14 \pm 0.65$	
CS0194	ATCDF5 J032928.59-283618.8	1.00	1.00	6.09	<	
CS0215	ATCDF5 J032950.01-273152.6	1.00	1.00	1.10	<	
CS0241	ATCDF5 J033010.21-282653.0	1.00	1.53	1.28	<	
CS0255	ATCDF5 J033024.08-275658.7	1.18	3.16	0.55	$1.91 \pm 0.53$	
CS0275	ATCDF5 J033043.69-284755.6	1.38	1.82	0.36	<	
CS0283	ATCDF5 J033048.68-274445.3	1.15	2.03	0.29	<	Not detected by Huynh et al. (2010)
CS0415	ATCDF5 J033213.07-274351.0	1.00	1.00	1.21	<	Not detected by Huynh et al. (2010)
CS0446	ATCDF5 J033231.54-280433.5	2.21	3.64	0.34	<	Detected by Huynh et al. (2010)
CS0487	ATCDF5 J033301.19-284720.7	1.00	1.59	1.12	<	Maybe not an IFRS: see Middelberg et al. (2011)
CS0506	ATCDF5 J033311.48-280319.0	1.56	2.36	0.17	<	Detected by Huynh et al. (2010)
CS0538	ATCDF5 J033330.20-283511.1	1.44	2.57	1.40	<	
CS0588	ATCDF5 J033404.70-284501.7	1.28	3.31	0.45	<	
CS0682	ATCDF5 J033518.48-275742.2	1.18	2.87	0.34	<	
CS0694	ATCDF5 J033525.08-273313.2	1.00	1.39	0.60	<	
CS0696	ATCDF5 J033525.25-283105.2	1.00	1.77	0.31	<	
CS0703	ATCDF5 J033531.02-272702.2	1.00	1.00	26.08	<	Polarized source: see Middelberg et al. (2011)
CS0706	ATCDF5 J033533.22-280621.8	1.05	1.50	0.26	<	
CS0714	ATCDF5 J033538.16-274400.6	1.44	2.21	0.39	<	

**Notes.** Columns 3 and 4 give the positional uncertainties described in Section 2. The measured 3.6  $\mu$ m flux densities are given in Column 6 with a formal uncertainty to the fitted aperture photometry. A < in Column 6 indicates that no peak was visible in the SERVS data within the radio position error ellipse, and the word *out* indicates that the source was outside the region observed with SERVS.

(2008) calculate the density of sources with  $S_{3.6 \mu\text{m}} > 1.1 \mu\text{Jy}$  as  $205,000 \text{ deg}^{-2}$ , from which we estimate that we should detect  $\sim 4$  sources by chance. This is greater than the number detected in the shifted data, but the difference is clearly dominated by small number statistics. Nevertheless, the Barmby result does provide a useful rough cross-check on our shifting technique.

In summary, of our 39 IFRSs which lie within the SERVS fields, we find that only 3 of these have a source within the radio position error ellipse, none has a measured flux density greater than five times the formal fitting uncertainty, and our basic Monte Carlo simulations suggest that most or all of these detections are due to chance. We conclude that few or none of our sources have reliable detections and the vast majority of

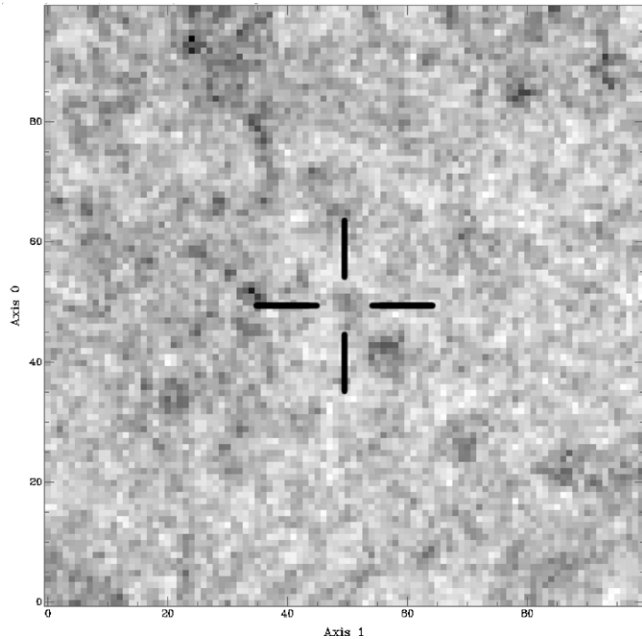


**Figure 3.**  $3.6\ \mu\text{m}$  median stacked image of the IFRSs, obtained by calculating the median of 39 images extracted from the SERVS  $3.6\ \mu\text{m}$  data, centered on the IFRS radio positions. The rms noise of the image is  $0.14\ \mu\text{Jy}$ , and the marginal detection at the center has a flux density (measured using aperture photometry) of  $0.21 \pm 0.14\ \mu\text{Jy}$ . Both axes are in units of pixels, each of which is  $0.6 \times 0.6$  arcsec.

IFRSs are undetected at this level. Such faint emission from a source which is relatively strong at radio wavelengths represents an extreme condition which is not common in the local universe.

The  $S_{3.6\ \mu\text{m}}$  distribution of IFRS can be explored to even deeper levels by stacking  $3.6\ \mu\text{m}$  images at the IFRS positions. In Figure 3, we show a median stacked image obtained by summing 39  $3.6\ \mu\text{m}$  images extracted from the SERVS data, centered on the IFRS radio position. Because the stacking has reached the confusion limit for these data, the rms noise no longer scales as the square root of integration time, and so the rms of this stacked image is higher than would be obtained in an unconfused field, although it still offers a significant improvement over the individual images. We note that Garn & Alexander (2008) faced a similar challenge in stacking  $3.6\ \mu\text{m}$  data from eight IFRS in the FLS, reaching a noise of approximately  $1\ \mu\text{Jy}$  in the image stack.

The measured rms of the median stacked image is  $0.14\ \mu\text{Jy}$ , and there is marginal evidence for a source at the field center whose flux density was measured to be  $0.21 \pm 0.14\ \mu\text{Jy}$ . Using a  $3\sigma$  upper limit, we conclude that the IFRSs have a median flux density of  $\lesssim 0.63\ \mu\text{Jy}$  at  $3.6\ \mu\text{m}$ .

### 3. RADIO/IR PROPERTIES OF IFRSs

Since we have no redshift information for any of the IFRSs, we focus here on two derived quantities: the ratio of  $S_{20\ \text{cm}}$  and  $S_{3.6\ \mu\text{m}}$ , or its lower limit, and the  $S_{3.6\ \mu\text{m}}$  flux density, or its upper limit.

Of the 39 IFRSs which lie within the SERVS fields, we find that, after allowing for confusion, only 1 or 2 are detected and none have a measured flux density greater than five times the formal fitting uncertainty. The remaining sources are undetected at this level. From this we deduce that the vast majority of IFRSs have a ratio of  $S_{20\ \text{cm}}$  to  $S_{3.6\ \mu\text{m}}$  in the range 200–2000.

In Figure 4, we show the ratios of  $S_{20\ \text{cm}}$  to  $S_{3.6\ \mu\text{m}}$  as a function of redshift for a representative selection of models and mark the

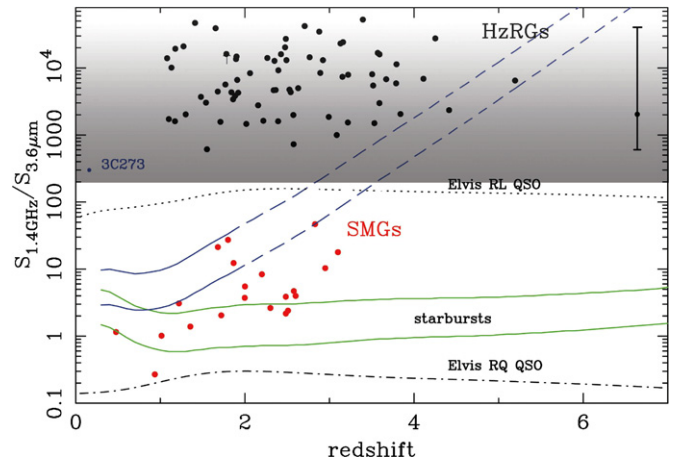


**Figure 4.** Ratios of 20 cm to  $3.6\ \mu\text{m}$  flux densities as a function of redshift, for a representative selection of models. The gray area represents the range of ratios for the individual IFRSs discussed in this paper. The dots within that area are the high-redshift radio galaxies studied by Seymour et al. (2007). The solid green lines indicate the expected loci of LIRG and ULIRG galaxies (using the template from Rieke et al. 2009) and the dotted (dot-dashed) line indicates the loci of a classical radio-loud (radio-quiet) QSO (from Elvis et al. 1994). The location of classical submillimeter galaxies is indicated by the red dots. The error bar on the right marks the likely range of the stacked image (obtained by dividing the range of radio flux densities of the IFRS by the flux density of the marginal detection in the stacked  $3.6\ \mu\text{m}$  image). The filled circle in the error bar represents the median radio flux density divided by the median  $3.6\ \mu\text{m}$  flux density. We note that dust extinction could cause any of the calculated tracks to rise steeply at high redshift, where the observed  $3.6\ \mu\text{m}$  emission is generated in visible wavelengths in the galaxy rest frame. This is illustrated by the blue lines which show the effect of adding  $A_v = 10$  mag of extinction to the two starburst tracks. The blue lines are dashed at high redshift to indicate that the radio emission from these galaxies would be undetectable at  $z > 2$  with current sensitivity.

(A color version of this figure is available in the online journal.)

limits obtained in this paper. It is clear from this figure that the only objects known to have such a high ratio are radio-loud AGNs, such as the HzRGs. In particular, we can rule out any known type of galaxy powered predominantly by star formation, such as ULIRGs, SMGs, etc., all of which fall well below the region occupied by IFRSs.

If they are radio galaxies similar to those in the low-redshift universe, then we can use their brightness to obtain constraints on redshift. In Figure 5, we show the  $S_{3.6\ \mu\text{m}}$  of HzRGs as a function of redshift, together with the limits obtained from our SERVS observations. The HzRGs follow a relation between redshift and  $S_{3.6\ \mu\text{m}}$  similar to the well-known  $K-z$  relation for other radio galaxies (Willott et al. 2003). Although we caution that both these relationships are unreliable above  $z > 3$ , they imply that if the IFRSs are radio galaxies, then their low  $3.6\ \mu\text{m}$  flux densities constrain them to lie at high redshift.

### 4. WHAT ARE IFRSs?

Whatever the nature of IFRSs, their properties are extreme and not consistent with any of the well-recognized classes of object. Here we review the options for what this class of object is likely to be.

1. *Star-forming galaxies.* Figure 4 shows that no known class of galaxy powered predominantly by star formation, such as ULIRGs, SMGs, etc., have ratios of 20 cm– $3.6\ \mu\text{m}$  flux densities comparable with those of IFRS. A star-forming galaxy might appear in the region if it suffered from an unusually high extinction, but no star-forming galaxy is

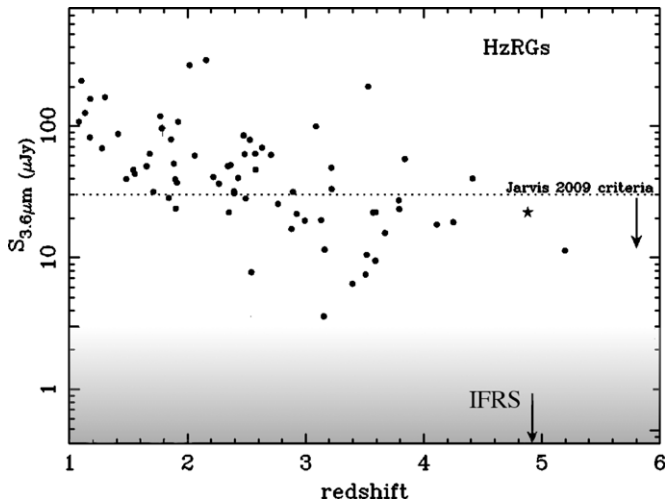


**Figure 5.**  $3.6\ \mu\text{m}$  flux densities of various classes of source as a function of redshift. The gray area represents the range of flux densities for the IFRSs discussed in this paper. The dots above it are the high-redshift radio galaxies studied by Seymour et al. (2007). The star represents the  $z = 4.88$  radio galaxy discovered by Jarvis et al. (2009), and the line represents the criterion used by Jarvis et al. to select their candidate high-redshift galaxies. The flux density of the stacked image,  $0.21\ \mu\text{Jy}$ , falls off the bottom of this diagram, as indicated by the arrow next to the IFRS label. We note that dust extinction could cause the HzRGs to fall to lower values of  $3.6\ \mu\text{m}$  flux density at high redshift, where the observed  $3.6\ \mu\text{m}$  emission is generated in visible wavelengths in the galaxy rest frame.

known with such high extinction. Even Arp 220 has an  $S_{20\text{cm}}/S_{3.6\ \mu\text{m}}$  ratio a factor of 20 below the most moderate IFRS, and a factor of 4000 below the most extreme IFRS.

Such high extinction could in principle be found in a star-forming galaxy if it were at high redshift ( $z > 3$ ), where the observed  $3.6\ \mu\text{m}$  emission is generated in visible wavelengths in the galaxy rest frame. However, no known star-forming galaxy generates sufficient radio power to reproduce the observed IFRS flux density. For example, Arp 220 at  $z = 3$  would have an observed flux of  $\sim 5\ \mu\text{Jy}$ .

The observed 20 cm radio luminosities of the IFRSs range from  $7 \times 10^{23}\ \text{WHz}^{-1}$  (for the weakest IFRS at  $z = 1$ ) to  $1.4 \times 10^{26}\ \text{WHz}^{-1}$  at  $z = 1$  to  $7 \times 10^{27}\ \text{WHz}^{-1}$  (for the strongest IFRS at  $z = 5$ ). The most luminous star-forming galaxies, typified by SMGs at  $z \sim 2-3$ , can have luminosities  $\sim 10^{24}\ \text{WHz}^{-1}$  (e.g., Ivison et al. 1998; Seymour et al. 2009), so that while the faintest of our galaxies could be caused by star-forming galaxies, most are too radio luminous.

In addition, two of the six IFRSs observed with VLBI were detected by Norris et al. (2007) and Middelberg et al. (2008a). The VLBI detections rule out star formation in these particular galaxies as the radio emission mechanism, since the synchrotron emission from star-forming galaxies rarely has sufficient brightness temperature to be detectable with VLBI (e.g., Kewley et al. 2000; Biggs et al. 2010).

Furthermore, Middelberg et al. (2011) and Banfield et al. (2011) show that the radio emission from several of the IFRSs studied by them is significantly polarized. This also argues against star formation, in which polarization is generally much lower than in AGNs.

We conclude that the majority of IFRSs are unlikely to represent star-forming galaxies.

2. *Radio lobes.* An early hypothesis was that IFRSs might be the extended radio lobes of an AGN whose host may be

located some distance away. The VLBI detections by Norris et al. (2007) and Middelberg et al. (2008a) imply that at least about a third of IFRSs have high brightness temperature cores, which rules out the possibility that they are radio lobes of AGNs, since radio lobes do not have sufficient surface brightness to be detectable with these VLBI observations. Furthermore, most IFRSs are unresolved in the high-resolution observations by Middelberg et al. (2011), making it unlikely that they are extended radio lobes.

3. *Pulsars.* Cameron et al. (2011) tested the hypothesis that IFRSs may be pulsars, by performing a pulsar search on a sample of IFRSs. Their results show that any putative pulsars in the field have a pulsed flux density well below the observed flux density of the IFRSs, and they conclude that the IFRSs are not radio pulsars.
4. *Radio-loud AGNs.* The extreme values of the ratio of  $S_{20\text{cm}}$  to  $S_{3.6\ \mu\text{m}}$  reported in Figure 4 are known to occur in radio-loud AGNs and have not been observed in any other type of extragalactic object. All the available observations (radio/IR flux densities, radio/IR ratio, VLBI, polarization) are consistent with the cores of radio-loud AGNs, and we conclude that radio-loud AGNs are therefore a natural explanation of IFRS.

If IFRSs are caused by radio-loud AGNs, their remaining unusual aspect is the extreme faintness at  $3.6\ \mu\text{m}$ . We now consider the following three possible causes.

1. *Dwarf galaxies that host a radio-loud AGN.* If a radio-loud AGN were to be hosted by a dwarf galaxy at moderate redshift, then the low luminosity of the host galaxy could reproduce both the faint  $3.6\ \mu\text{m}$  flux density and the high  $S_{20\text{cm}}$  to  $S_{3.6\ \mu\text{m}}$  ratio of the IFRS. However, such objects are observationally unknown, and theoretically unlikely given the weak potential well of a dwarf galaxy.
2. *Moderate-redshift radio-loud AGN with heavy dust extinction.* Figure 5 shows that a known moderate-redshift ( $z \lesssim 3$ ) AGN would be detected in our  $3.6\ \mu\text{m}$  observations. We can postulate moderate-redshift objects which are heavily obscured at  $3.6\ \mu\text{m}$ , but the amounts of extinction required are very high. For example, 3C 273 at  $z = 1$  would require an extinction of  $A_V \sim 50^m$  to occupy the position of IFRSs in Figure 5. On the other hand, at high redshift ( $z > 2$ ), where the observed  $3.6\ \mu\text{m}$  emission is generated in visible wavelengths in the galaxy rest-frame, as little as  $A_V = 10$  mag of extinction is sufficient to raise the track of a radio-loud QSO into the regime of the IFRS.

However, even if the AGN is obscured by dust, it is hard to obscure the host galaxy to the low  $3.6\ \mu\text{m}$  flux limits presented here. Even in Arp 220, where as much as 100 mag of extinction obscure the nucleus (e.g., Haas et al. 2001), the outer shell of the host galaxy is still bright at IR wavelengths. To reproduce the extreme IR-faintness of the IFRS, the extinction must cover the entire body of the galaxy.

We therefore cannot exclude the possibility that the IFRSs could be a new class of galaxy at  $z \sim 1-2$ , in which the entire galaxy must be shrouded in dust, reducing its integrated  $3.6\ \mu\text{m}$  flux density by a factor of 100.

3. *High-redshift radio-loud AGNs.* Figure 5 and the  $K-z$  relation show that, if IFRSs belong to a parent population similar to that of known radio-loud AGNs, they must lie at  $z \geq 3$ . We note that obscured HzRGs and quasars have been detected by Martínez-Sansigre et al. (2006),

Dey et al. (2008), Yan et al. (2007), and Sajina et al. (2007). While IFRSs bear some similarities to these galaxies, IFRSs are even more extreme in their  $S_{20\text{ cm}}$  to  $S_{3.6\ \mu\text{m}}$  ratios. For example, Martínez-Sansigre et al. (2006) choose their sample by requiring that  $S_{3.6\ \mu\text{m}} < 45\ \mu\text{Jy}$ , while the IFRSs have  $S_{3.6\ \mu\text{m}} \lesssim 1\ \mu\text{Jy}$ . While none of the IFRSs are detected at  $24\ \mu\text{m}$ , the available SWIRE data at  $24\ \mu\text{m}$  are relatively insensitive compared to the  $3.6\ \mu\text{m}$  SERVS data, and, given the very low  $S_{3.6\ \mu\text{m}}$ , only a very extreme spectral energy distribution would enable them to be detected at  $24\ \mu\text{m}$ .

We conclude that the most natural explanation for IFRSs is that they are very similar to known classes of radio-loud AGNs, but at a redshift  $\geq 3$ . In all these properties, the IFRSs most resemble the HzRGs of Seymour et al. (2007), Ivison et al. (2008), and Jarvis et al. (2009), but with even more extreme  $20\text{ cm}$ – $3.6\ \mu\text{m}$  flux density ratios. However, we cannot exclude the possibility that they are a new class of lower-redshift ( $1 < z < 3$ ) radio-loud AGNs in which the luminosity of the entire host galaxy is reduced by a factor of  $\sim 100$  by dust extinction.

The  $20\text{ cm}$  flux densities of our IFRSs range from 0.14 to 26 mJy. The weakest end of the range corresponds to a luminosity  $7 \times 10^{23}\ \text{WHz}^{-1}$  at  $z = 1$  to  $4 \times 10^{25}\ \text{WHz}^{-1}$  at  $z = 5$ , giving it the luminosity of an FR I galaxy at any reasonable redshift. On the other hand, the brightest end of the range corresponds to a luminosity  $1.4 \times 10^{26}\ \text{WHz}^{-1}$  at  $z = 1$  to  $7 \times 10^{27}\ \text{WHz}^{-1}$  at  $z = 5$ , making it an FR II galaxy at any reasonable redshift. Thus the class of IFRSs spans both the FR I and FR II luminosity classes, with the majority of galaxies straddling the FR I/FR II break, depending on their redshift.

It would be instructive to consider these results in terms of black hole mass,  $M_{\text{BH}}$ , but Snellen et al. (2003) have shown that there is no good correlation between radio luminosity and black hole mass for radio-loud galaxies and so we cannot estimate a black hole mass except in the most general terms. But we do have good observational evidence for the  $3.6\ \mu\text{m}$  flux densities of host galaxies of HzRGs, which is shown in Figure 5.

We have detected 51 IFRSs in the  $7\ \text{deg}^2$  area of ATLAS, implying a density of IFRSs on the sky of  $\sim 7\ \text{per deg}^2$  for  $S_{20\text{ cm}} > 0.1\ \text{mJy}$ . It is difficult to make a meaningful comparison of the numbers of IFRSs with source counts at the present time without a better constraint on redshift. The SKADS simulation (Wilman et al. 2008) gives a sky density of 0.5 FR II galaxies  $\text{deg}^{-2}$  at  $z \gtrsim 4$ , implying that only 3–4 of the IFRSs discussed here are FR II galaxies at  $z \gtrsim 4$ . However, the space density of all but the highest-luminosity, FR II-type radio sources are very poorly constrained at high redshifts, and AGN models are very poorly constrained by current observations at the low flux densities probed here. Thus it is possible (Zinn et al. 2011) that the IFRSs could be radio-loud AGNs of moderate radio luminosity and much higher space density than their more powerful counterparts.

## 5. CONCLUSION

We have searched for IR counterparts to 39 IR-faint radio sources using deep  $3.6\ \mu\text{m}$  observations from SERVS. Even though the sensitivity is 3–5 times better than the previous observations (with SWIRE), few or none of the IFRSs are detected after taking into account the number of chance associations, and a stacked image indicates a median  $3.6\ \mu\text{m}$  flux density of  $0.21 \pm 0.14\ \mu\text{Jy}$ . This places extreme constraints on the properties of these sources, making it likely that they are radio-loud

AGNs at redshifts  $z \gtrsim 3$ , or heavily dust-obscured radio-loud AGNs at redshifts  $z \gtrsim 1$ . While some may have radio-to-IR ratios similar to 3C 273, but at a much higher redshift, the most extreme of them require several magnitudes of obscuration in the optical/NIR to remain undetected by deep imaging.

While we cannot rule out the possibility that more than one type of object may be represented by IFRSs, the evidence suggests that a significant proportion, if not all, of the IFRSs are either

1. radio-loud AGNs (similar to known high-redshift radio-loud AGNs) at  $z \gtrsim 3$  or
2. a new class of lower-redshift ( $1 < z < 3$ ) radio-loud AGNs in which the luminosity of the entire host galaxy is severely reduced by dust extinction.

This work is based in part on observations made with *Spitzer*, which is operated by the Jet Propulsion Laboratory, California Institute of Technology under a contract with NASA. Support for this work was provided by NASA through an award issued by JPL/Caltech. This research has made use of the NASA/IPAC Extragalactic Database (NED) which is operated by the Jet Propulsion Laboratory, California Institute of Technology, under contract with the National Aeronautics and Space Administration. The Australia Telescope is funded by the Commonwealth of Australia for operation as a National Facility managed by CSIRO. J.A. gratefully acknowledges the support from the Science and Technology Foundation (FCT, Portugal) through the research grant PTDC/FIS/100170/2008. M.Y.M. acknowledges the support of an Australian Postgraduate Award as well as Postgraduate Scholarships from AAO and ATNF.

We thank P. Barmby for providing unpublished details of her source density calculations, Barnaby Norris for generating the stacked median image, and George Hobbs for helpful comments on the pulsar density at high galactic latitude.

## REFERENCES

- Banfield, J. K., George, S. J., Taylor, A. R., Stil, J. M., Kothes, R., & Scott, D. 2011, *ApJ*, **733**, 69
- Barmby, P., Huang, J.-S., Ashby, M. L. N., Eisenhardt, P. R. M., Fazio, G. G., Willner, S. P., & Wright, E. L. 2008, *ApJS*, **177**, 431
- Biggs, A. D., Younger, J. D., & Ivison, R. J. 2010, *MNRAS*, **408**, 342
- Cameron, A. D., Keith, M., Hobbs, G., Norris, R. P., Mao, M. Y., & Middelberg, E. 2011, *MNRAS*, in press
- De Breuck, C., van Breugel, W., Stanford, S. A., Röttgering, H., Miley, G., & Stern, D. 2002, *AJ*, **123**, 637
- Dey, A., et al. 2008, *ApJ*, **677**, 943
- Elvis, M., et al. 1994, *ApJS*, **95**, 1
- Garn, T., & Alexander, P. 2008, *MNRAS*, **391**, 1000
- Haas, M., Klaas, U., Müller, S. A. H., Chini, R., & Coulson, I. 2001, *A&A*, **367**, L9
- Higdon, J. L., Higdon, S. J. U., Willner, S. P., Brown, M. J. I., Stern, D., Le Floch, E., & Eisenhardt, P. 2008, *ApJ*, **688**, 885
- Higdon, J. L., et al. 2005, *ApJ*, **626**, 58
- Huynh, M. T., Norris, R. P., & Middelberg, M. 2010, *ApJ*, **710**, 698
- Ivison, R. J., Smail, I., Le Borgne, J.-F., Blain, A. W., Kneib, J.-P., Bezecourt, J., Kerr, T. H., & Davies, J. K. 1998, *MNRAS*, **298**, 583
- Ivison, R. J., et al. 2007, *MNRAS*, **380**, 199
- Ivison, R. J., et al. 2008, *MNRAS*, **390**, 1117
- Jarvis, M. J., Rawlings, S., Eales, S., Blundell, K. M., Bunker, A. J., Croft, S., McLure, R. J., & Willott, C. J. 2001, *MNRAS*, **326**, 1585
- Jarvis, M. J., Teimourian, H., Simpson, C., Smith, D. J. B., Rawlings, S., & Bonfield, D. 2009, *MNRAS*, **398**, L83
- Kewley, L. J., Heisler, C. A., Dopita, M. A., Sutherland, R., Norris, R. P., Reynolds, J., & Lumsden, S. 2000, *ApJ*, **530**, 704
- Lonsdale, C., et al. 2004, *ApJS*, **154**, 54
- Martínez-Sansigre, A., Rawlings, S., Lacy, M., Fadda, D., Jarvis, M. J., Marleau, F. R., Simpson, C., & Willott, C. J. 2006, *MNRAS*, **370**, 1479

- Mauduit, M., et al. 2011, *ApJ*, submitted
- Middelberg, E., Norris, R. P., Hales, C. A., Seymour, N., Johnston-Hollitt, M., Huynh, M. T., Lenc, E., & Mao, M. Y. 2011, *A&A*, **526**, A8
- Middelberg, E., Norris, R. P., Tingay, S., Mao, M. Y., Phillips, C. J., & Hotan, A. W. 2008a, *A&A*, **491**, 435
- Middelberg, E., et al. 2008b, *AJ*, **135**, 1276
- Norris, R. P., Tingay, S., Phillips, C., Middelberg, E., Deller, A., & Appleton, P. N. 2007, *MNRAS*, **378**, 1434
- Norris, R. P., et al. 2006, *AJ*, **132**, 2409
- Rieke, G. H., Alonso-Herrero, A., Weiner, B. J., Pérez-González, P. G., Blaylock, M., Donley, J. L., & Marcillac, D. 2009, *ApJ*, **692**, 556
- Sajina, A., Yan, L., Lacy, M., & Huynh, M. 2007, *ApJ*, **667**, L17
- Scoville, N., et al. 2007, *ApJS*, **172**, 1
- Seymour, N., Huynh, M., Dwelly, T., Symeonidis, M., Hopkins, A., McHardy, I. M., Page, M. J., & Rieke, G. 2009, *MNRAS*, **398**, 1573
- Seymour, N., et al. 2007, *ApJS*, **171**, 353
- Smail, I., Ivison, R. J., & Blain, A. W. 1997, *ApJ*, **490**, L5
- Snellen, I. A. G., Lehnert, M. D., Bremer, M. N., & Schilizzi, R. T. 2003, *MNRAS*, **342**, 889
- Surace, J., et al. 2005, SWIRE Data Delivery Document, NASA-IPAC
- Willott, C. J., Rawlings, S., Jarvis, M. J., & Blundell, K. M. 2003, *MNRAS*, **339**, 173
- Wilman, R. J., et al. 2008, *MNRAS*, **388**, 1335
- Yan, L., et al. 2007, *ApJ*, **658**, 778
- Zinn, P.-C., Middelberg, E., & Ibar, E. 2011, *A&A*, in press